Numerical study on two-point contact by an explicit integration finite element method
A contribution to the modeling of flange squeal

Yang, Zhen; Li, Zili; Dollevoet, Rolf

Important note
To cite this publication, please use the final published version (if applicable).
Please check the document version above.

Numerical study on two-point contact by an explicit integration finite element method – A contribution to the modeling of flange squeal

Zhen Yang*, **Zili Li and Rolf Dollevoet**
Delft University of Technology, Section of Railway Engineering
Stevinweg 1, 2628 CN, Delft, the Netherlands
* e-mail: Z.Yang-1@tudelft.nl

ABSTRACT
The precise mechanism which activates squeal, especially flange squeal has not been fully explained. The complex non-Hertzian contact and the broad-band high frequency feature bring great challenges to the modelling work of flange squeal. In this paper, an explicit integration finite element method is presented to simulate the dynamic curving behavior of the outer wheel, which is believed directly related to flange squeal generation. By fully considering the normal, tangential force and spin moment, the non-steady-state wheel-rail interaction from one-point to two-point contact is reproduced. The critical time step of the explicit integration scheme is determined by the Courant stability condition, which, together with the detailed modelling of the structural and continuum of the wheel/track system, effectively guarantees that the reproduced vibration frequency can reach up to 10 kHz with desired accuracy. The aim of the work is to contribute to the modelling and understanding of the generation mechanism of the flange squeal from the viewpoint of the wheel-rail interaction.

1. INTRODUCTION

Squeal noise may occur when a railway vehicle negotiates tight curves. Since the leading wheelset fails to align itself tangentially to the rail, high lateral creepage happens at the contact between the tread of the inner wheel and the top surface of the low rail, and the flange of the outer wheel is in contact with the gauge corner of the high rail. During this process, two types of high frequency curve squeal effects, namely the tonal 'wheel squeal' and the more broad-band 'flange squeal', although sharing some features, can be excited by the inner and the outer wheel-rail interactions, respectively.

Systematical study on curve squeal noise started in the 1970s, when Rudd described the wheel-rail frictional characteristic (the functional dependence between friction force and wheel-rail relative velocity) in terms of 'negative damping' (generalized as full 'stick-slip') and attribute it to the mechanism of wheel squeal [1]. Since then, various increasingly sophisticated theoretical models adopted parts of this mechanism and were developed from Rudd's seminal model [2-7].

Compared to wheel squeal, much less attention has been paid to the study of flange squeal [8-9], consciously or unconsciously. On one hand, the complex non-Hertzian contact, which combines wheel-rail penetration, creepage and spin motion, and the broad-band high frequency feature (5 kHz-10 kHz [10]) bring great challenges to the modelling work. On the other hand, many researchers believe that the intermittent flange squeal plays a minor role because it has a lower level than wheel squeal and the flange contact may reduce the likelihood and level of wheel squeal of inner wheel to some extent [2]. Nevertheless, this believe is challenged by measurements performed in Australia, which shows that no benefit is gained by applying friction modifier to the low rail only, but the noise can be reduced significantly by lubricating the gauge corner region of high rail [11].

Due to the fact that the acting force between the wheel flange and the rail gauge corner, including normal load, creep force and spin moment, can be resolved into vertical direction and lateral direction [8], the flange rubbing may simultaneously excite both radial and axial vibration modes of wheel. As noted by Thompson [12], the radial modes and one-nodal-circle axial modes of wheel have similar resonant frequencies, making them easily coupled with each other. The 'mode coupling dynamic instability' or so-called 'sprag-slip' mechanism is thus employed complementarily with 'negative damping' theories for flange squeal prediction [7,13,14]. To tackle the arbitrary contact in wheel squeal and flange squeal study, Kalker's theory of rolling contact is widely adopted [3,4,7,13,15]. Although these improved approaches take both the tangential and normal dynamics into account, there are still field observations often failed to be explained by the existing theories [16], indicating that the precise mechanism which activates squeal, especially flange squeal has not been fully explained.

2. SCOPE AND METHOD OF THIS PAPER

It is believed a combined numerical treatment of both the vehicle dynamics and the friction-induced squeal is

unreasonable because of the large difference in the time-scales and the frequency ranges [14]. The squeal study can thus be broken down into a quasi-static part imposed by vehicle dynamics and a dynamic part caused by unstable wheel vibration [13]. The previous contact models, rigorous or simplified, basically rely on the wheel/rail contact position and angle of attack pre-calculated by the quasi-steady-state curving behavior model as input parameters to predict the occurrence of squeal [3,4,7,13-15].

Strictly speaking, when two-point contact is involved, the wheel curving behavior may not be fully considered as being in quasi-steady state. Instead, it can be divided into three stages, and the corresponding contact forms are shown schematically in Fig. 1. Stages 1 and 3, respectively represents the period before and after the change of wheel-rail contact, during which the wheel-rail interaction with either one-point or two-point contact can be regarded as in a quasi-steady state; while in stage 2, as the wheel flange approaches and comes in touch with the gauge corner, a transition from one-point contact to two-point contact takes place. With the transfer of the normal load from rail top to gauge corner, the wheel is lifted gradually and a subsequent transition from two-point to one-point (stage 3, lower figure) contact may also happen. The wheel-rail interaction in this transition process is non-steady. At the end of the transition, the relative position of the wheel and the rail stabilizes with either two-point or one-point (only at gauge corner) contact, so that steady-state curving begins.
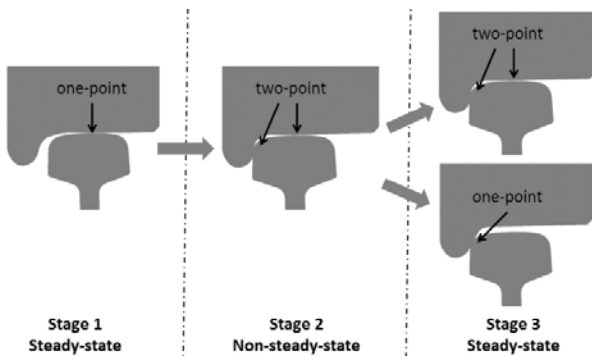

Fig. 1. Wheel-rail contact form in 3 stages of wheel curving behavior

The squeal phenomenon is characterized as 'enigmatic' [16] or 'erratic' [14, 17], because of the large fluctuations observed in the occurrence of squeal, the noise levels and the squeal wheel modes in practice even for apparently identical conditions [18]. It is suggested that the non-steady-state irregular motion of wheel (in stage 2 of Fig. 1), determining the contact position and orientation of wheel at the entry of the quasi-steady-stage curving behavior (in stage 3 of Fig. 1), can significantly affect the occurrence and degree of squeal [4].

In this regard, this paper is concentrated on the wheel-rail contact during the non-steady-state transition from one-point to two-point. The aim is to provide a better understanding and preparation for the next step modelling of flange squeal.

The approach presented in this paper, namely an explicit integration finite element method, has been proven to be effective and accurate for solving the frictional rolling contact between wheel tread and rail head [19], which corresponds to the one-point contact in stage 1. The method can take into account the normal load, the creep force as well as the moment due to spin for arbitrary contact geometry. Compared with Kalker's algorithms, the FE method drops the half-space assumption; Moreover, the transient dynamic behavior, which is directly related to squeal generation [20], can be fully considered with the method; Further, material properties more complex than linear elasticity can be dealt with in future study to propose new materials for noise reduction. The integration is performed in the time domain with an explicit central difference scheme, owing to that: The regularization problem caused by the no-slip condition in the adhesion area of contact patch can be avoided and the computing efficiency is considerably improved when the high frequency vibration has to be considered [21].

3. MODELLING AND VALIDATION OF THE WHEEL MODES

As shown in Fig. 2 (a), a 3D finite element (FE) transient wheel-track interaction model is developed, in which a 10 m length of half-side track and a half wheel set with sprung mass of the car body and the bogie are considered. The wheel, the rail and the sleepers are modelled with 8-node solid elements. In order to achieve a high accuracy of the solution with a reasonable model size, non-uniform meshing scheme is used. The mesh size around the initial position of the wheel-rail contact and the 150 mm length of solution zone is 1 mm. The lumped mass of the car body and bogie are modelled as mass elements, connected to the wheelset by the primary suspension of the vehicle with parallel linear springs and viscous dampers. Since the substructure has little influence on the high-frequency dynamic behavior studied in this paper, each sleeper only contains 12 solid elements and the ballast is simplified as vertical spring and damper elements with the displacements constrained in lateral and longitudinal directions. The parameters involved in the track model are mainly taken from [22]. The wheel-rail contact is defined with real geometry including the contact between wheel flange and rail gauge corner, seen in Fig. 2 (b), enabling the creepage and the spin motion caused by the flange rubbing to be fully taken into account. The wheel geometry corresponds to a passenger car wheel of the Dutch railway network with the standard profile of S1002; The rail is modeled as the UIC54E1 with an inclination of 1:40. The constant friction coefficient is set to 0.6.

(a) Full FE model

(b) Wheel-rail profile/interaction
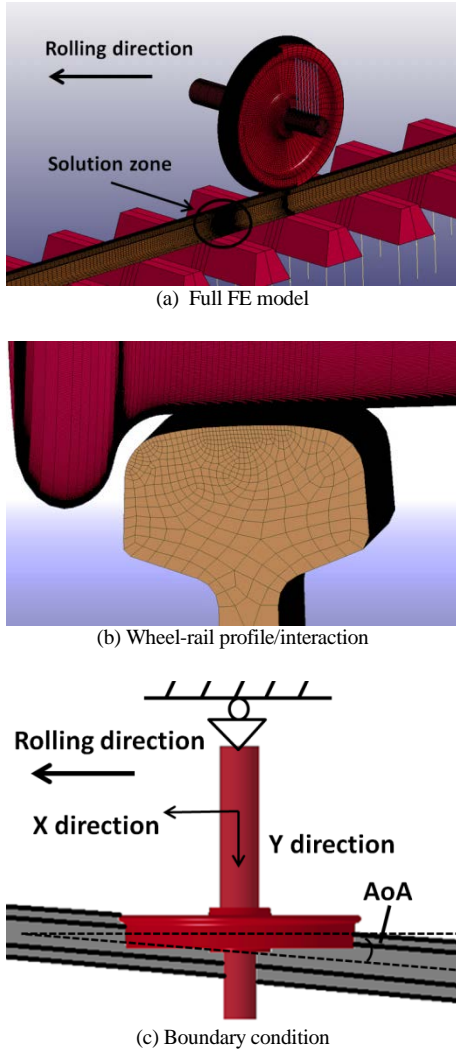

(c) Boundary condition

Fig. 2. Wheel-rail interaction model

The non-steady-state wheel curving behavior is achieved in the model by applying the boundary condition to the wheel in the way shown in Fig. 2 (c). The lateral displacement is constrained at the inner side of wheel axle and the outer end of the axle is free. In the transient dynamic simulation, a dynamic relaxation is first employed to make the system reach an equilibrium state under gravity. The movements of the wheel in both rotation and forward translation are applied as the initial conditions. The wheel is subsequently driven by a proper rotational torque applied on the axle, consequently exerting a longitudinal creep force between wheel and rail, which satisfies that the traction coefficient is below the friction coefficient. The wheel is set to roll in the presence of friction from the initial position toward the solution zone with a speed of 80 km/h along the X direction, forming an angle of attack (AoA) with respect to the rail longitudinal direction. The effects of transient wheel rotation can thus be included inherently.

In the initial stage of the simulation, the wheel-rail contact occurs only between rail top and wheel tread. The contact patch is determined with the normal nodal force: A node is in contact if the absolute value of the normal nodal force is non-zero. The yellow area shown

in Fig. 3 (a) is the rail surface in the solution zone. The origin of the coordinate is at the center of rail bottom surface at the initial position of the wheel-rail contact. Note that the coordinate already includes the rail inclination in the track. A trail of blue patches on it represents the 'footprints' of the contact at a series of time steps under one-point contact situation. Due to the AoA, the wheel flange moves towards the gauge corner as the time step goes on and the 2nd contact patch starts to appear. The 'footprints' of the contact patches in the case of two-point contact are shown as two trails of red patches, respectively, on the rail top and the gauge corner. The coordinates of the wheel/rail nodes in and around the circled two contact patches (labelled as 'patch 1' and 'patch 2' in Fig. 3 (a)) from a same time step are plotted in Fig. 3 (b). The contact angle within the range of 'patch 2' is roughly between 65° and 75°.

(a) Contact patches on the rail

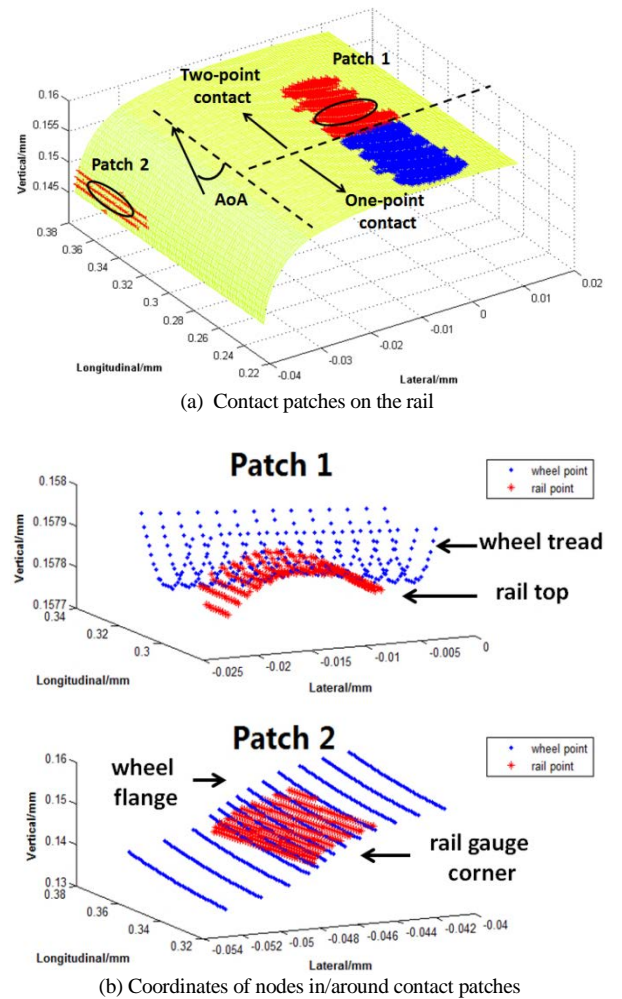(b) Coordinates of nodes in/around contact patches

Fig. 3. Contact patches in the solution zone

In the transient dynamic simulation, the integration is performed in the time domain with an explicit central difference scheme. Very small time step (86 ns) is employed for the model to meet Courant stability condition [23]. This, together with the detailed modelling of the structural and continuum of the wheel/track system, effectively guarantees that high frequency dynamic effect up to 10 kHz is reproduced.

Each tone frequency of squeal is expected to be related to a wheel mode [17, 24]. All the physical vibration modes of the wheel within the frequency range of squeal (10 kHz) is identified by the FE wheel model in Fig. 2 (a) but with the inner edge of the hub clamped, which can adequately represent the dynamics of the wheel under contact with the rail [14]. The wheel modal frequencies in 3 dimensions of axial, radial and circumferential are plotted in Fig. 4. A good agreement is observed by comparing the calculated results with the experimental modal frequency of the NS-intercity wheel up to 5 kHz from [12], which has the same or similar wheel type as the one modelled here.
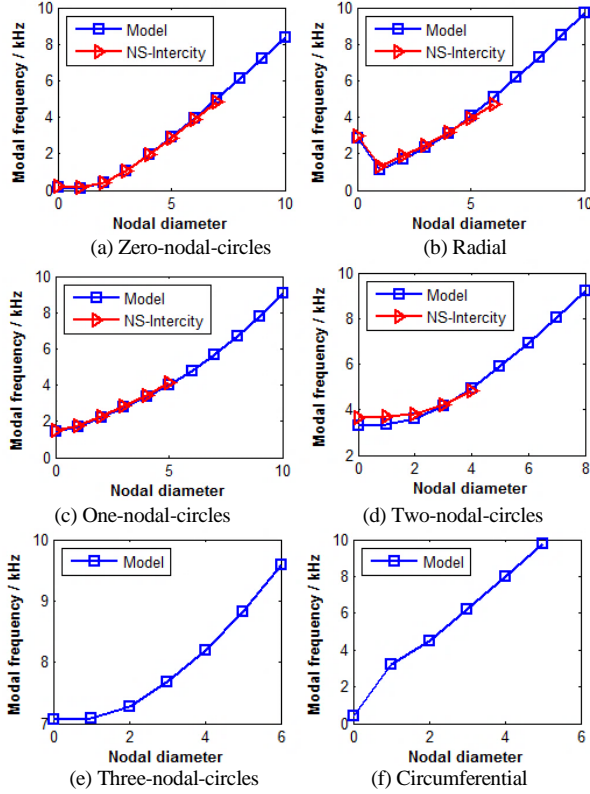

Fig. 4. Validation of the wheel modes calculated by FE model

4. SOLUTION OF THE CONTACT MODEL

The FE solutions of the one-point contact problem between rail top and wheel tread in both the normal and the longitudinal directions have been verified in [19] by comparing with Hertz and CONTACT solutions. The work presented in this paper extends the solution to two-point contact with application to the study of flange squeal. The emphasis is on the character of the distribution of adhesion-slip area, shear stress magnitude and direction in the contact patch, which are believed to be closely associated to the frictional instability of squealing wheel.

4.1.   Transition from One-point to Two-point Contact

Before flanging takes place, it is one point contact between the wheel and rail (stage 1 in Fig. 1). Fig. 5 gives the calculated distribution of adhesion-slip area and the normal/shear stress along the longitudinal axis

of a typical contact patch (with AoA = 20 mrad). Whether a node is in adhesion or not is determined by comparing the value $F_{nn} \times f$ - F_{nt} with a tolerance ε_T, where F_{nn}, F_{nt} and f refers to the nodal force in the direction normal to the local surface, in the tangential direction and friction coefficient respectively, and ε_T is set as a percentage of the largest tangential nodal force in the contact area as in [19]. The values in Fig. 5 (a) equal to $F_{nn} \times f$ - F_{nt}, and the unit of the legend on the right side is 'newton'. The upper bound is assigned to the values greater than it (the red region) and its inverse is set as the lower bound to manifest the nodes out of the contact patch (the blue region). The predicted range of the adhesion area is indicated with the oval in Fig. 5 (a), which is located at the leading part of the contact patch. The distribution of adhesion-slip area along longitudinal axis can also be obtained from the stress distribution graph in Fig. 5 (b). The normal and shear stresses, hereinafter plotted in the stress distribution graphs and referred as F_n and F_t in the legend, are extracted from the center line of contact patches along the longitudinal direction. The adhesion-slip areas indicated in Fig. 5 (a) and (b) agree with each other and are proven reasonable by comparing them with the corresponding results in [19], qualifying the model for the following two-point contact study.

(a) Adhesion-slip area distribution

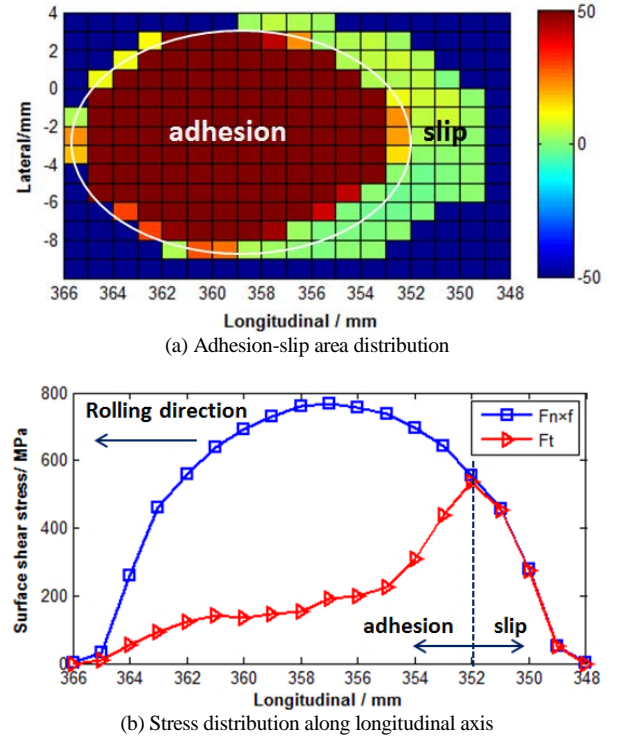(b) Stress distribution along longitudinal axis

Fig. 5. One-point contact condition

When the wheel proceeds along the rail with the given AoA, two-point contact occurs (stage 2 in Fig. 1). Fig. 6 shows the calculated adhesion-slip area distribution during the transition from one-point to two-point contact. The abscissa of the figures indicates that the contact patch shown in Fig.6 (a), (b) and (c) comes out successively. In Fig. 6 (a),   the 2nd contact patch (between wheel flange and rail gauge corner, shown in the lower graph) has just come into being and its size is

small, compared to the ones in (b) and (c). The 1st contact patch (between wheel tread and rail top, shown in the upper graph) looks similar to that of one-point contact in Fig. 5. From (a) to (b) and to (c), with the progress of transition, the size of the adhesion area in patch 1, indicated with the ovals in the figures, decreases and it moves gradually from the leading part of contact patch to the center. This change of the contact patch can also be seen from the stress distribution shown in Fig. 7.

The graphs in the lower row in Fig. 6 and Fig. 7 show that the majority of nodes in the patch 2 are in slip, namely $F_{nn} \times f = F_{nt}$ according to the Coulomb's law employed in the model. A few nodes in adhesion, indicated with the ovals, appear on the upper edge of

patch 2 and their amount gradually increases with the flange climbing.

In the non-steady-state transition of wheel-rail interaction, the adhesion-slip area distribution of the contact patches are changing continuously in Fig. 6 and Fig. 7. In reality, the non-steady state may last for certain time and then tend to become steady to enter stage 3 when the inertial effect of the wheel curving motion is compensated. A more realistic boundary condition is required for the model in the next step to investigate at which moment the steady state will be achieved and how the contact may affect the subsequent frictional instability of wheel.
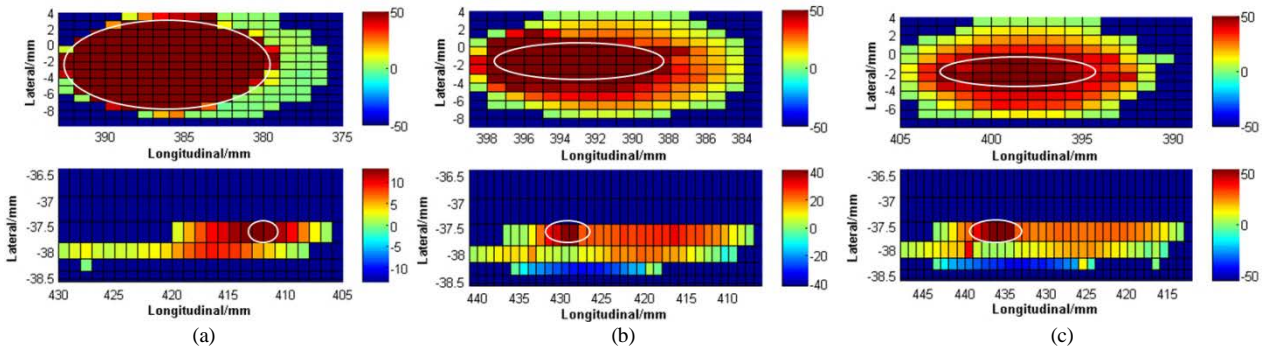

Fig. 6. Adhesion-slip area distribution of two-point contact condition (upper graphs: patch 1; bottom graphs: patch 2)
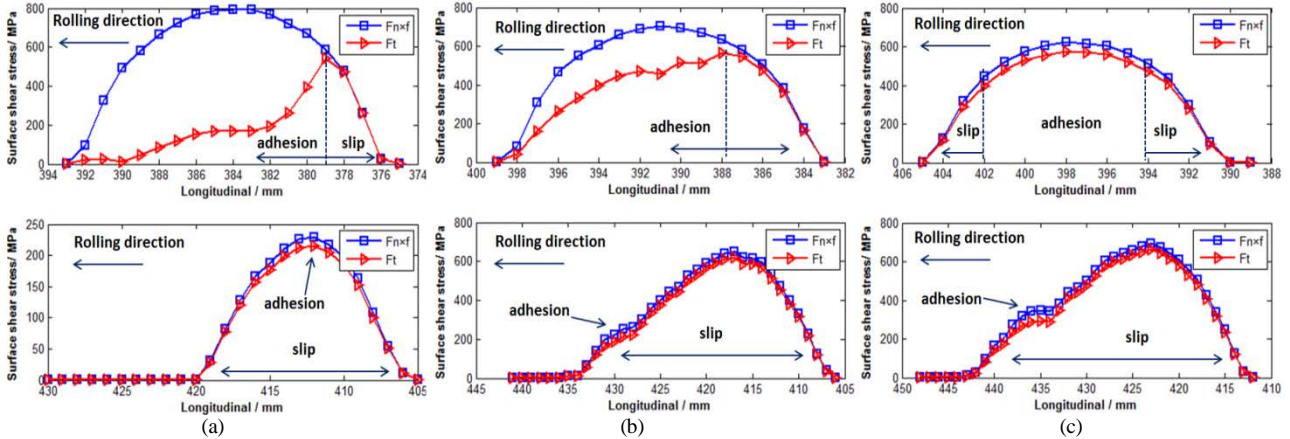

Fig. 7. Stress distribution along longitudinal axis of two-point contact condition (upper graphs: patch 1; bottom graphs: patch 2)

4.2. Shear Stress Direction

The stress distributions along the longitudinal axis shown in Fig. 5 and Fig. 7 only indicate the magnitudes of the normal and shear stresses. In order to present the direction of the shear stress, their distributions in the contact patches corresponding to Fig. 6 are plotted in the vector diagrams of Fig. 8. The arrows inside the patches point in the direction of the shear stress and their length is proportional to the magnitude. The

orientation angle between the vector of shear stress and the negative direction of longitudinal axis in patch 1 and patch 2 are noted as $\theta 1$ and $\theta 2$, respectively, labelled in Fig. 8 (b), to characterize the shear stress direction in the contact patch. From Fig. 8, the overall trend can be observed that $\theta 1$ increases during the transition process; while $\theta 2$ generally remains stable. The change of the orientation of shear stress substantially results from the magnitude changes of shear stress in lateral and longitudinal directions.
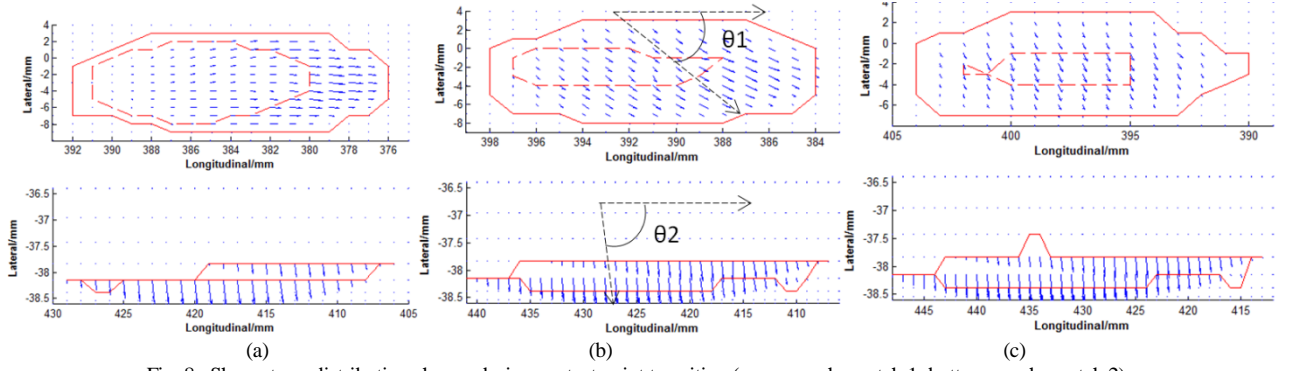
Fig. 8. Shear stress distribution change during contact point transition (upper graphs: patch 1; bottom graphs: patch 2)

AoA is generally thought as one of the key factors in the occurrence of squeal [16]. To investigate the influence of AoA on the shear stress change during the contact transition, the specific changes of the shear stress magnitude in the lateral and longitudinal directions, as well as angles $\theta1$ and $\theta2$ with different AoA are shown in Fig. 9. The value in Fig. 9 is the average of all elements within the contact patch. The abscissas of the figures is the contact patch number, corresponding to the sequence of the output time step (0.3 ms for each). It can be seen that for all the 3 simulation cases, the calculated lateral shear stress (upper row in Fig. 9) dramatically grows with the presence of patch 2 and that of patch 2 is larger than patch 1. In the middle row, the longitudinal shear stress of patch 1 declines to certain extent because of the participation of patch 2. The bottom row presents that the absolute value of $\theta1$ keeps in the range of less than 20° in the stage of one-point contact. It jumps to approximate 70° in 2-3 output time steps once patch 2 appears. The orientation angle $\theta2$ maintains at a high value between 60° and 70° as soon as it appears.

By comparing the shear stresses under the 3 AoA conditions in Fig. 9, it can be seen, as for the patch 2, the lateral shear stress increases but the longitudinal one decreases with the increase of AoA, consequently causing the rise of $\theta2$; No pronounced influence of AoA on shear stress of patch 1 is observed from the simulation, except that the longitudinal shear stress is slightly raised by applying a larger AoA.

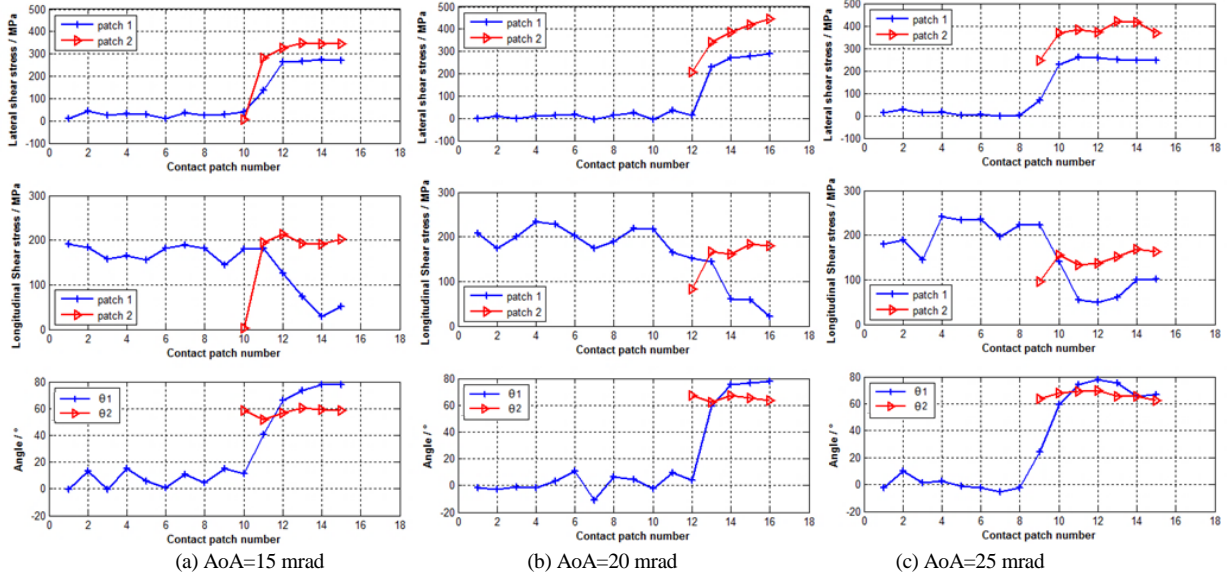(a) AoA=15 mrad   (b) AoA=20 mrad   (c) AoA=25 mrad

Fig. 9. The change of shear stress and orientation with different AoA
(upper graphs: lateral stress; middle graphs: longitudinal stress; bottom graphs: orientation angle)

5. CONCLUSIONS AND FUTURE WORK

The non-steady-state rolling contact with the transition from one-point to two-point is simulated in this paper by an explicit integration finite element method. The adhesion-slip area distribution, surface stress magnitudes and shear stress direction under one-point and two-point contact conditions, as well as the influences of AoA are studied. The wheel modes and contact-related results predicted by the FE model are proven reasonable when comparing to the measurement and calculation results in the literature,

laying a solid foundation for the next step flange squeal simulation.

The remaining work is concerned mainly with the reproduction of the flange squeal by extending the simulation from the non-steady-state contact point transition to the steady-state two-point or one-point (flange/gauge corner) contact condition. The boundary condition needs to be adjusted in order to create a quasi-steady-state wheel curving motion after the occurrence of two-point contact. With the modified model, the influence of the wheel-rail contact form,

position and orientation of wheel motion on flange squeal and the relation between wheel modal frequency and squeal tone frequency are going to be investigated.

6. REFERENCES

[1] Rudd, M.J.: Wheel/rail noise - Part II: Wheel squeal. Journal of Sound and Vibration. 46(3), 381–394 (1976).

[2] Remington, P.J.: Wheel/rail squeal and impact noise: What do we know? What don't we know? Where do we go from here?. Journal of Sound and Vibration. 116(2), 339–353 (1985).

[3] Fingberg, U.: A model of wheel-rail squealing noise. Journal of Sound and Vibration. 143(3), 365-377 (1990).

[4] Periard, F.J.: Wheel-Rail Noise Generation: Curve Squealing by Trams. PhD Thesis, Delft University of Technology, The Netherlands, 1998.

[5] Heckl, M.A. Abrahams, I.D.: Curve squeal of train wheels, Part I: Mathematical model for its generation. Journal of Sound and Vibration. 229(3), 669–693 (2000).

[6] De Beer, F.G. Janssens, M.H.A.: Squeal noise of rail-bound vehicles influenced by lateral contact position. Journal of Sound and Vibration. 267, 497–507 (2003).

[7] Huang, Z.Y.: Theoretical modelling of railway curve squeal. PhD thesis, University of Southampton, 2007.

[8] Thompson, D.J. Jones, C.J.C.: Noise and Vibration from Railway Vehicles, Handbook of Railway Vehicle Dynamics. Taylor & Francis Group, LLC, 2006.

[9] Anderson, D. Wheatley, N.: Mitigation of Wheel Squeal and Flanging Noise on the Australian Rail Network. Notes on Numerical Fluid Mechanics and Multidisciplinary Design. 99, 399-405 (2008).

[10] Eadie, D. Santoro, M. Kalousek, J.: Railway noise and the effect of top of rail liquid friction modifiers: changes in sound and vibration spectral distribution in curves. Wear. 258, 1148-1155 (2005).

[11] Curley, D. Anderson, D. C. Jiang, J. Hanson, D. Field trials of gauge face lubrication and top-of-rail friction modification for curve noise mitigation. Notes on Numerical Fluid Mechanics and Multidisciplinary Design. 126, 449-456 (2015).

[12] Thompson, D.J.: Railway Noise and Vibration : Mechanisms, Modelling and Means of Control. Elsevier, 2009.

[13] Chiello, O. Ayasse, J.B. Vincent, N. Koch, J.R.: Curve squeal of urban rolling stock- Part 3: Theoretical model. Journal of Sound and Vibration. 293, 710-727 (2006).

[14] Glocker, Ch. Cataldi-Spinola, E. Leine, R.I.: Curve squealing of trains: Measurement, modelling and simulation. Journal of Sound and Vibration. 324, 365-386 (2009).

[15] Pieringer, A. Kropp, W.: Modelling of railway curve squeal including effects of wheel rotation. Notes on Numerical Fluid Mechanics and Multidisciplinary Design. 126, 417-424 (2015).

[16] Jiang, J. Anderson, D. Dwight, R. The mechanisms of curve squeal. Notes on Numerical Fluid Mechanics and Multidisciplinary Design. 126, 587-594 (2015).

[17] Vincent, N. Koch, J.R. Chollet, H. Guerder, J.Y.: Curve squeal of urban rolling stock-Part 1: State of the art and field measurements. Journal of Sound and Vibration. 293, 691-700 (2006).

[18] Thompson, D.J. Jones, C.J.C.: A review of the modelling of wheel/rail noise generation. Journal of Sound and Vibration. 231(3), 519–536 (2000).

[19] Zhao, X. Li, Z.: The solution of frictional wheel-rail rolling contact with a 3D transient finite element model: Validation and error analysis. Wear. 271, 444-452 (2011).

[20] Huang, Z.Y. Thompson, D.J. Jones, C.J.C.: Squeal prediction for a bogied vehicle in a curve. Notes on Numerical Fluid Mechanics and Multidisciplinary Design. 99, 313-319 (2008).

[21] Li, Z.: Numerical solution of wheel-rail rolling contact- some recent results, application and unsolved problems. Proceedings of 9th International Conference on Contact Mechanics and Wear of Rail/Wheel Systems, Chengdu (China). 72-78 (2012).

[22] Zhao, X. Li, Z. Liu, J.: Wheel-rail impact and the dynamic forces at discrete supports of rails in the presence of singular rail surface defects, Rail and Rapid Transit. 226, 124-139 (2011).

[23] Courant, R. Friedrichs, K. Lewy, H. On the partial difference equations of mathematical physics. IBM Journal of Research and Development. 11(2), 215-234 (1967).

[24] Squicciarini, G. Usberti, S. Thompson, D.J. Corradi, R. and Barbera, A.: Curve squeal in the presence of two wheel/rail contact points. Notes on Numerical Fluid Mechanics and Multidisciplinary Design. 126, 603-610 (2015).